

# New insights into the structure-nonlinear mechanical property relations for graphene allotropes



Hao Sun <sup>a,1</sup>, Sankha Mukherjee <sup>b,1</sup>, Matthew Daly <sup>b</sup>, Ajay Krishnan <sup>c</sup>,  
Manohar Harsha Karigerasi <sup>d</sup>, Chandra Veer Singh <sup>a,b,\*</sup>

<sup>a</sup> Department of Mechanical and Industrial Engineering, University of Toronto, Toronto, ON, M5S 3G8, Canada

<sup>b</sup> Department of Materials Science and Engineering, University of Toronto, Toronto, ON, M5S 3E4, Canada

<sup>c</sup> Department of Metallurgical and Materials Engineering, National Institute of Technology Karnataka, Surathkal, 575025, India

<sup>d</sup> Department of Metallurgical and Materials Engineering, Indian Institute of Technology Roorkee, Roorkee, Uttarakhand, 247667, India

## ARTICLE INFO

### Article history:

Received 19 April 2016

Received in revised form

14 August 2016

Accepted 7 September 2016

Available online 10 September 2016

## ABSTRACT

A vast array of two-dimensional (2D) graphene allotropes have been reported to possess remarkable electronic, thermal, and magnetic properties. However, our understanding of their structure-mechanical-property relationship is far from complete. In this study, we performed extensive density functional theory calculations to evaluate the mechanical properties of 11 different graphene allotropes, comprising structures with solely  $sp^2$  hybridized bonds and both  $sp$  and  $sp^2$  hybridized bonds. A complete set of nonlinear anisotropic elastic constants up to the fifth order are determined for these structures. Energetics of the deformation of these allotropes have been analyzed to mathematically establish a relationship between the sum of the second order nonlinear elastic constants and the area density. Empirical relationships have been obtained for predicting the Young's moduli, Poisson's ratios and the ultimate tensile strengths (UTS) of the allotropes using their area densities and the sizes of the carbon rings. Furthermore, comparison with traditional engineering materials reveals that 2D graphene allotropes expand the available material-property space by occupying a new region with both high Young's modulus and a high UTS, as well as a high UTS and low density.

© 2016 Elsevier Ltd. All rights reserved.

## 1. Introduction

The expanding library of two-dimensional (2D) materials has provided access to an ever-increasing source of tailored material properties at the monolayer length-scale. 2D graphene allotropes represent a family of graphene-like materials whose topological variants result in material properties outside the envelope established for graphene. While graphene is known to be one of the strongest materials ever synthesized, with a Young's modulus ( $E$ ) and ultimate tensile strength (UTS) of 1 TPa and 118 GPa [1], respectively, its poor ductility limits the usability for certain applications. On the other hand, several graphene allotropes possess certain useful properties. For example, graphyne exhibits direction-dependent Dirac cones [2]; C65 and C64 have higher hydrogen

binding energies than graphene [3]; graphene allotropes with pentagonal rings, such as (PentaHexocite [4], C65 [5]) show ferromagnetically polarized electron spin [6]. These unique properties can be utilized to design nanotubes, nanoribbons, and other low-dimensional nanomaterials for novel applications. For instance, the family of graphyne-based nanotubes can be both metallic and semiconducting depending on the orientation (i.e. armchair or zigzag) [7]. Similarly, nanotubes created using Penta-Hexocite possess chirality-dependent electronic and mechanical properties due to its pentagonal carbon rings [4]. Furthermore, when an entire W-Net-Octagraphene sheet is cut into ribbons of certain widths, semiconductivity is introduced [8]. Since these intriguing properties essentially arise from the topological arrangement of different carbon rings, an in-depth understanding of their structure-property relationship is critical for effective screening and practical applications.

Previous studies concerning the mechanical properties of graphene allotropes, such as the family of graphyne (graphyne [9–11], graphdiyne [9,12], graphtriyne [9], and graphtetrayne [9]), Gr10

\* Corresponding author. Department of Mechanical and Industrial Engineering, University of Toronto, Toronto, ON, M5S 3G8, Canada.

E-mail address: [chandraveer.singh@utoronto.ca](mailto:chandraveer.singh@utoronto.ca) (C.V. Singh).

<sup>1</sup> These authors contributed equally to this work.

**Table 1**  
Structural and bonding information for all the graphene allotropes studied here.

Graphene allotropes	Nature of bonding	Area density $\text{\AA}^{-2}$	Carbon rings	Reference
Gr11	$sp^2$	0.256	C3, C12	Enyashin et al. [19]
Octagraphene (OcGr)	$sp^2$	0.336	C4, C8	Sheng et al. [20]
C64-Graphenylene (C64)	$sp^2$	0.303	C4, C6, C12	Song et al. [21]
C41	$sp^2$	0.358	C4, C7	Lu et al. [5]
W Net Octagraphene (NetW)	$sp^2$	0.359	C8, C6, C4	Wang et al. [22]
PentaHexoctite (PHexOct)	$sp^2$	0.360	C8, C5, C6	Sharma et al. [4]
C65	$sp^2$	0.351	C9, C5, C6	Lu et al. [5]
C31	$sp^2$	0.313	C9, C3	Lu et al. [5]
Graphene	$sp^2$	0.384	C6	Novoselov [23]
Graphyne	$sp+sp^2$	0.292	C6, C12	Baughman et al. [20]
Supergraphene (Gr10)	$sp+sp^2$	0.190	C18	Baughman et al. [20]
Squarographene 13' (SqGr13)	$sp+sp^2$	0.345	C6, C10	Bucknum et al. [24]

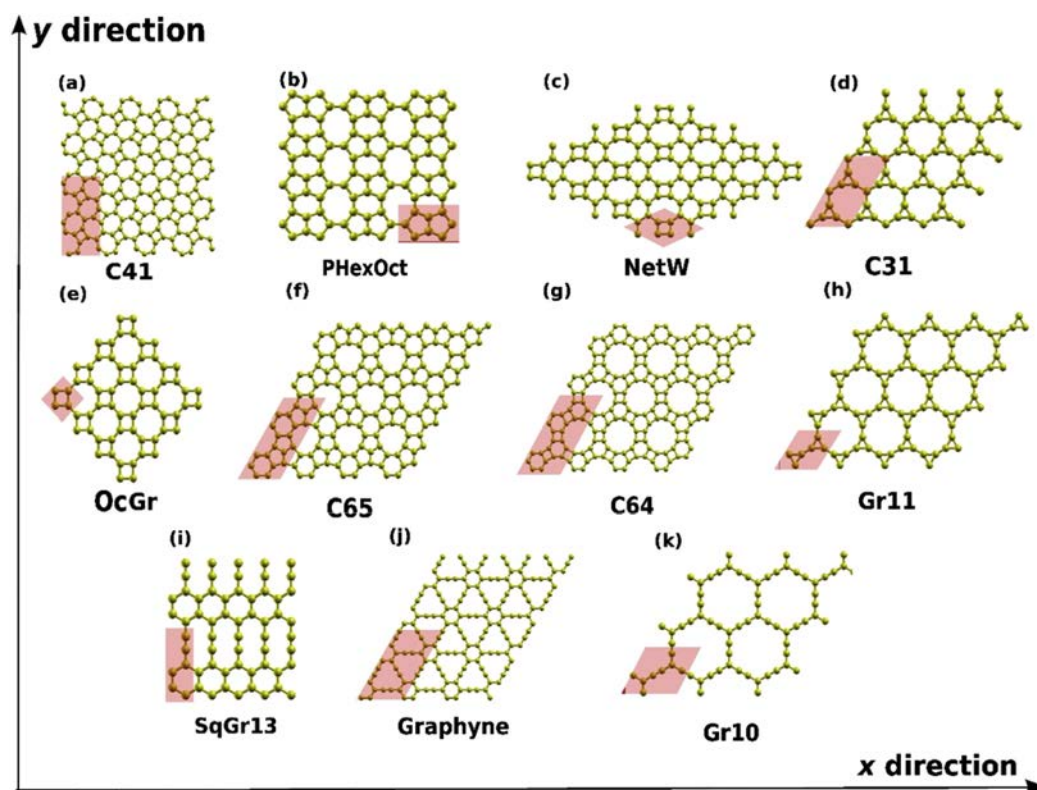


**Fig. 1.** Atomic topologies for the examined graphene allotropes. The periodic unit cells are highlighted in pink. (a) to (h) contain only  $sp^2$  bond, while (i) to (k) contain both  $sp$  and  $sp^2$  bonds. (A colour version of this figure can be viewed online.)

[13], Gr11 [13], octagraphene (OcGr) [14], pentaheptite [14], have reported nonlinear stress-strain relationships and brittle fracture. Theoretical calculations predict that the Young's moduli and UTS of the graphene allotropes mentioned above are much lower than pristine graphene [9,14]. However, interestingly, an enhancement in ductility is also observed for some allotropes which have a low area density of atoms (here area density is defined as the number of carbon atoms per unit area) [9]. Certainly the mechanical properties of the allotropes will depend on: (a) the strength of the C-C bond, and (b) the topological arrangement of the atoms. Previous studies have reported that the area and bond densities [9,15] play a crucial role in determining the Young's modulus and Poisson's ratio of the carbon allotropes. Cranford et al. [9] found that for the structures within the graphyne family, the stiffness and the UTS decreases as the percentage of  $sp$  hybridized bonds increases. However, the same effect is not valid for the wider realm of 2D

graphene allotropes without  $sp$  bonds. Fthenakisa et al. [14] theoretically studied three  $sp^2$  hybridized graphene allotropes (two pentaheptites and octagraphene) and found them to have a lower UTS and stiffness than graphene. However, one of these allotropes, Octagraphene (OcGr), has a higher failure strain than graphene. Furthermore, these structure-property relationships are obtained on a case-by-case basis, and lack physical insights.

Recently, the atomic structure and mechanical properties of carbyne, a new 1D carbon allotrope, have been investigated theoretically using *ab initio* simulations [16,17]. In these works, researchers identified relationships between the strength of the structure and the binding energy of the edge atom. Additionally, the effect of geometrical factors, such as the length of the carbyne, the bond length alternation between two nearby bonds in carbyne, and the C-C bond length on its mechanical properties were studied. A similar understanding of the structural-mechanical property

relationships in graphene allotropes is still missing.

In this manuscript, we present a comprehensive theoretical analysis of the structure and mechanical properties relations of 11 different graphene allotropes. The allotropes investigated herein were chosen to include a mix of different hybridizations, atomic area densities, ring patterns, and topological arrangements, thereby representing a vast array of possible atomic structures. To the best of our knowledge, the mechanical behavior of most of these allotropes, particularly the nonlinear stress-strain relations under varied loading conditions, have not been reported elsewhere. Using first-principle density functional theory (DFT) computations, we simulated the stress-strain responses under uniaxial and biaxial loading, and the complete set of anisotropic nonlinear elastic constants were estimated by fitting the stress-strain data to the fourth order polynomial based on continuum elasticity theory. Based on an in-depth analysis of the ground state energies of  $sp$  and  $sp^2$  hybridized C-C bonds during deformation, we obtained

structure-property relations for predicting the mechanical properties of graphene allotropes. Additionally, we compared the mechanical properties of the allotropes with traditional materials using Ashby Materials Selection Charts [18] to guide engineering design for future applications.

## 2. Methodology

Graphene allotropes represent topological variations of the hexagonal graphene structure through different tessellations of varied carbon rings. Table 1 summarizes the structural information of the allotropes studied herein, including their names, specifics of the carbon rings, and the area densities. The schematics of the allotropes are shown in Fig. 1. The structures studied include eight allotropes with  $sp^2$  hybridized C-C bonds comprising of 3-, 4-, 5-, 6-, 7-, 8-, 9-, 12-atom carbon rings (Fig. 1 a–h) and three allotropes with both  $sp^2$  hybridized and  $sp$  hybridized bonds (Fig. 1(i–k)). We

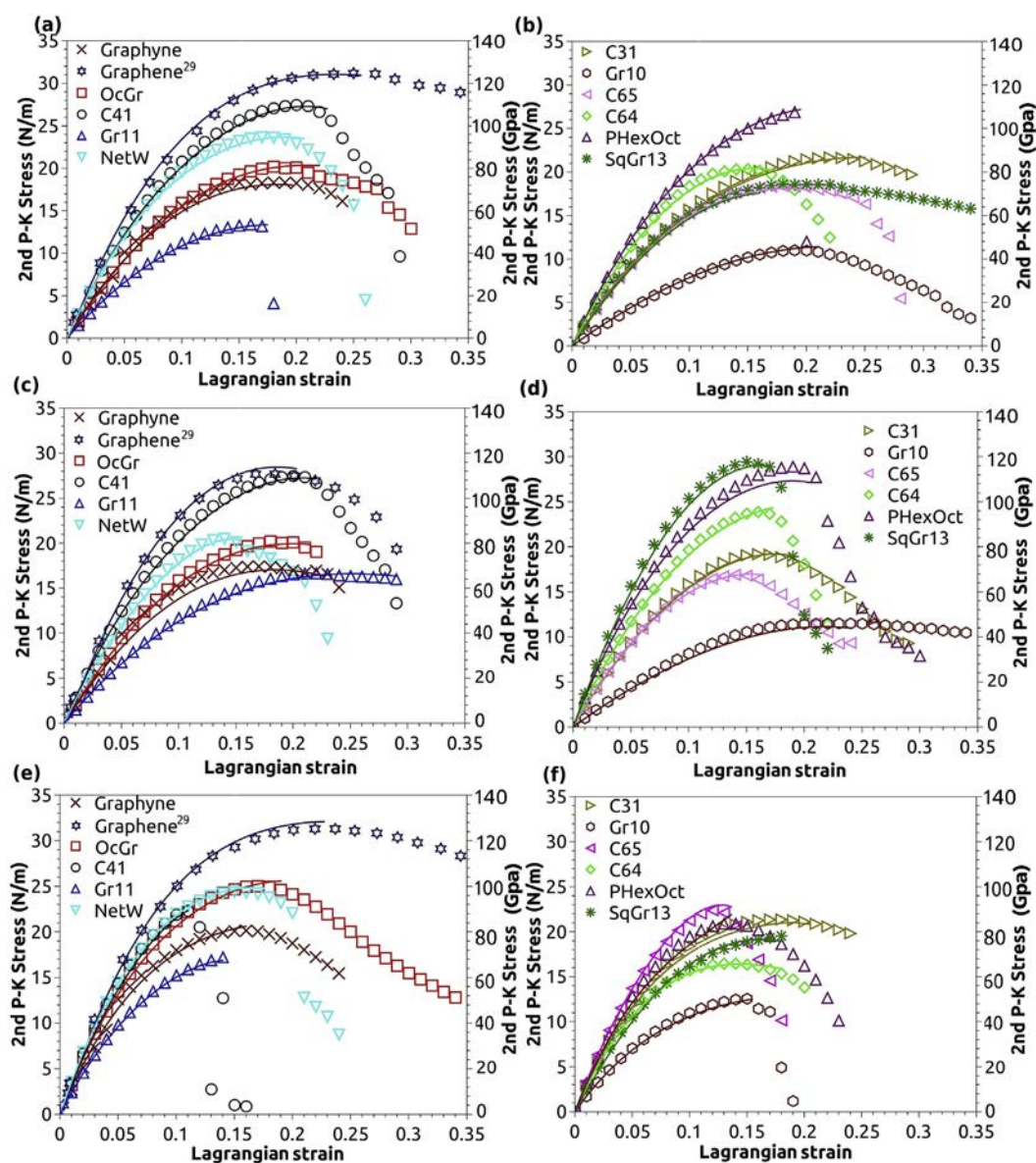


**Fig. 2.** Stress-strain curves for all allotropes, compared with graphene [29]. (a), (b) represent uniaxial tension in x direction; (c), (d) represent uniaxial tension in the y direction and (e), (f) in biaxial tension. The DFT data is marked by points, whereas solid lines represent the fitted continuum model as per Eqs. (2)–(10). (A colour version of this figure can be viewed online.)

used  $C_n$  notation to describe allotropes constructed from carbon rings of  $n$  atoms. For example, SqGr13 (Fig. 1(i)) is comprised of contiguous aromatic benzene rings (C6 with solely  $sp^2$  bonds) and 10-atom rings (C10 with both  $sp$  and  $sp^2$  bonds) which contain  $sp$  bonds [19]. Graphyne is composed of both aromatic benzene rings (C6) and weakly antiaromatic 12-membered rings (C12) with equal portions of both  $sp$  and  $sp^2$  hybridized bonds (Fig. 1(j)) [25]. Gr10 has 18-atom rings (C18) with both  $sp$  and  $sp^2$  hybridized bonds (Fig. 1(k)) [19].

Uniaxial and biaxial tensile simulations were performed on the unit cells illustrated in Fig. 1 using first principles DFT with a plane-wave basis set as implemented in the Quantum-ESPRESSO package [26]. The Generalized Gradient Approximation with the Perdew-Berke-Ernzerhof (PBE) pseudopotential [27] and a  $13 \times 13 \times 3$  k-point Monkhorst–Pack grid [28] were used for all calculations. The kinetic energy cut-offs of 60 and 480 Ry were used for the wavefunctions and charge density, respectively. The convergence criterion of the self-consistent field procedure was set to  $1.0 \times 10^{-6}$  Ry. There was a 20 Å vacuum in the out-of-plane direction to avoid any inter-layer interactions. Each system was initially relaxed using a conjugate gradient minimization method until the magnitude of the residual Hellmann–Feynman force on each atom was less than 0.001 Ry/Bohr. Subsequently, the cells were subjected to differing magnitudes of uniaxial and equal-biaxial strains in the  $x$  and  $y$  directions (see Fig. 1 for cell orientation). The strains were applied by dilating the unit cells along the loading direction and applying an equal affine transformation to the atomic positions. The deformed topology was then subjected to an energy minimization routine to obtain its ground state configuration. During this relaxation step, the cell dimensions were kept constant to preserve the overall strain on the deformed configuration. The true (Cauchy) stress ( $\sigma$ ) for prescribed levels of strain was obtained for each optimized structure from the pressure tensor. The 15 nonlinear elastic constants were evaluated for each allotrope by performing least-squares fitting of the stress-strain data using the fifth order continuum description of the nonlinear elasticity theory, proposed by Wei et al. [29]. The Cauchy stress was converted to the 2nd Piola-Kirchhoff (P-K) stress  $\Sigma$  through the deformation tensor ( $F$ ) using the relation [30]:

$$\Sigma = JF^{-1}\sigma(F^{-1})^T, \quad J = \det(F). \quad (1)$$

To obtain stress values in 2D terms with unit  $N/m$ , a 3.45 Å thickness was assumed for each allotrope [31], treating graphene as the reference material.

Following Ref. [29], the mechanical responses of the graphene allotropes under uniaxial Lagrangian strain ( $\eta$ ) along the  $x$  direction

(denoted by index 1  $\eta_1 \geq 0, \eta_2 = \eta_6 = 0$ ) can be represented using the Voigt notation by the following relation:

$$\sum_1^1 = C_{11}\eta_1 + \frac{1}{2}C_{111}\eta_1^2 + \frac{1}{6}C_{1111}\eta_1^3 + \frac{1}{24}C_{11111}\eta_1^4, \quad (2)$$

$$\sum_2^1 = C_{12}\eta_1 + \frac{1}{2}C_{112}\eta_1^2 + \frac{1}{6}C_{1112}\eta_1^3 + \frac{1}{24}C_{11112}\eta_1^4, \quad (3)$$

$$\sum_6^1 = 0. \quad (4)$$

For uniaxial loading along the  $y$  direction, where  $\eta_1 = 0, \eta_2 \geq 0, \eta_6 = 0$ , the mechanical response is given by:

$$\sum_1^2 = C_{12}\eta_2 + \frac{1}{2}(C_{111} - C_{222} + C_{112})\eta_2^2 + \frac{1}{12}(C_{1111} + 2C_{1112} - C_{2222})\eta_2^3 + \frac{1}{24}C_{12222}\eta_2^4, \quad (5)$$

$$\sum_2^2 = C_{22}\eta_2 + \frac{1}{2}C_{222}\eta_2^2 + \frac{1}{6}C_{2222}\eta_2^3 + \frac{1}{24}C_{22222}\eta_2^4, \quad (6)$$

$$\sum_6^2 = 0. \quad (7)$$

Under equi-biaxial loading, the constitutive equations are:

$$\begin{aligned} \sum_1^{biax} &= (C_{11} + C_{12})\eta + \frac{1}{2}(2C_{111} - C_{222} + 3C_{112})\eta^2 + \frac{1}{6}\left(\frac{3}{2}C_{1111} \right. \\ &\quad \left. + 4C_{1112} - \frac{1}{2}C_{2222} + 3C_{1122}\right)\eta^3 + \frac{1}{24}(3C_{11111} + 10C_{11112} \\ &\quad \left. - 5C_{12222} + 10C_{11122} - 2C_{22222})\eta^4, \end{aligned} \quad (8)$$

$$\sum_1^{biax} = \sum_2^{biax}, \quad (9)$$

**Table 2**  
UTS (N/m), corresponding  $\eta_u$ , Young's modulus  $E$  (N/m) and Poisson's ratio  $\nu$  for all allotropes.

	$x$ -UTS	$y$ -UTS	Biaxial UTS	$x$ - $\eta_u$	$y$ - $\eta_u$	Biaxial $\eta_u$	$\nu$	$E$ (N/m)
C41	27.5	27.5	22.3	0.21	0.21	0.12	0.29	272.9
OcGr	20.2	20.2	25	0.19	0.19	0.18	0.60	134.5
C64	18.4	16.9	16.5	0.19	0.15	0.14	0.27	210
Gr11	13.4	16.7	17.2	0.17	0.23	0.15	0.64	92.6
NetW	23.7	20.5	24.4	0.18	0.15	0.16	0.26	277.9
PHexOct	26.9	28.9	20.9	0.2	0.2	0.15	0.11	289.9
C65	20.3	23.9	22.4	0.16	0.17	0.13	0.26	257.2
C31	21.7	19.2	21.4	0.23	0.17	0.18	0.39	186.8
Graphene <sup>11</sup>	31.2	29.3	33.2	0.23	0.18	0.23	0.17	348.6
Graphyne	17.4	18.3	20.2	0.18	0.2	0.17	0.43	162.1
Gr10	11.5	11	12.6	0.24	0.2	0.16	0.86	26
SqGr13	18.6	29.4	19.5	0.19	0.16	0.18	0.14	<sup>a</sup>

<sup>a</sup> Anisotropic,  $x$ : 203.5  $y$ : 351.7.

**Table 3**  
Nonlinear elastic constants (N/m) of graphene and graphene allotropes.

Graphene allotropes	Second order nonlinear elastic constant			Third order nonlinear elastic constants			Fourth order nonlinear elastic constants				Fifth order nonlinear elastic constants			
	C <sub>12</sub>	C <sub>22</sub>	C <sub>11</sub>	C <sub>112</sub>	C <sub>222</sub>	C <sub>111</sub>	C <sub>1122</sub>	C <sub>1112</sub>	C <sub>2222</sub>	C <sub>1111</sub>	C <sub>22222</sub>	C <sub>12222</sub>	C <sub>11112</sub>	C <sub>11111</sub>
Graphene	60	358	358	-337	-2693	-2817	2583	759	10359	13416	-33447	-13047	-88	-31384
Gr11	98	152	154	-629	-830	-947	6211	4960	1687	666	1293	-14599	-30280	6262
OcGr	128	212	212	-826	-1078	-1090	4571	5237	-3009	-2567	48185	-25717	-25337	47707
C64	61	227	227	-529	-1785	-1792	1098	3176	8957	7735	-97340	-962	-22089	-27095
C41	87	298	299	-1094	-2467	-2501	16949	13209	20071	20725	-146150	-93029	-90592	-151040
NetW	79	273	299	-538	-2896	-2689	2736	4432	45587	18938	-645790	162310	-29514	-113940
PHexOct	31	335	293	-682	-2963	-2376	-2187	6881	22312	15015	-152950	-54365	-5720	-67730
C65	72	277	276	-405	-2010	-2273	10805	2485	11017	12610	-78642	5303	-15492	-119950
C31	86	220	220	-569	-1565	-1630	-232	5007	10282	8954	-116560	-41163	-31092	-35301
Graphyne	85	199	199	-873	-1264	-891	8662	4395	1154	-7966	14262	15495	-10393	89000
Gr10	83	94	97	-580	-369	-346	2040	4047	350	-986	-12835	-25790	-19728	1176
SqGr13	42	373	222											

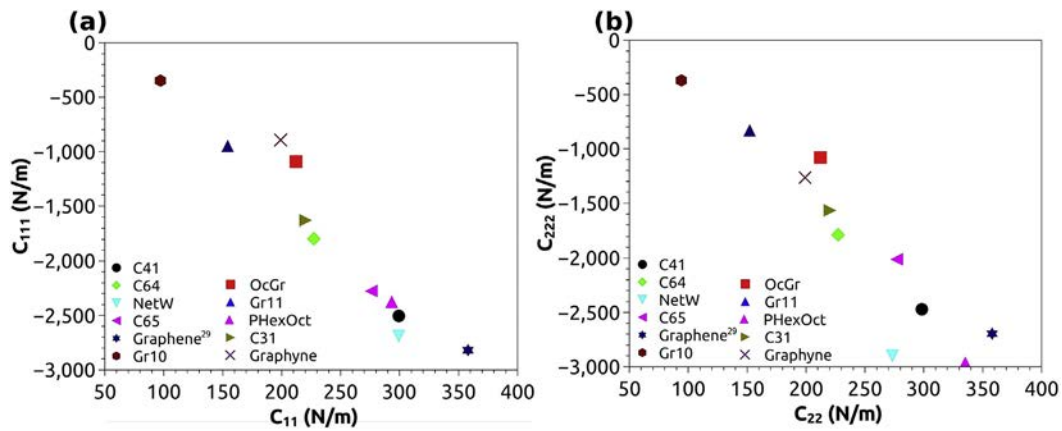


**Fig. 3.** The relation between the second order and third nonlinear elastic constants under (a) x-uniaxial, (b) y-uniaxial tension. SqGr13 is omitted here as it was not fit using the continuum model due to its anisotropy. (A colour version of this figure can be viewed online.)

$$\sum_6^{biax} = 0. \quad (10)$$

Eqs. (2), (3), (5), (6), (8) and (9) are valid for both infinitesimal and finite strains under arbitrary in-plane tensile loading, and have been implemented in other DFT-based quantum-mechanical simulations of graphene-based materials [10,29,32]. It is however important to note that in the study conducted by Wei et al. [29], Eq. (6) assumed  $C_{11} = C_{22}$ , which is not accurate for systems with significant mechanical anisotropy such as SqGr13. Since SqGr13 exhibits severe anisotropy, therefore, Eqs. (2), (3), (5), (6), (8) and (9) are not valid. For this allotrope, we obtained the second order nonlinear elastic constants by fitting the energy-strain curve. In the Supporting Information, we calculated the second order nonlinear elastic constants based on energy-strain curves for all the graphene allotropes. We found that except SqGr13, the nonlinear elastic constants calculated by energy-strain curves are exactly the same as that calculated by the above equations, which further prove the accuracy of our method.

### 3. Results and discussion

#### 3.1. Stress-strain responses

The 2nd P–K stress versus Lagrangian strain responses for the graphene allotropes studied are shown in Fig. 2. The stress-strain

responses (x-uniaxial tension, y-uniaxial tension, and biaxial tension) of graphene evaluated by Wei et al. [29] are also plotted in Fig. 2 (a), (c), and (e), respectively, for comparison. Our simulations show that for all the graphene allotropes, nonlinear relationships between the stress and strain exist. Additionally, strain softening takes place for Lagrangian strains larger than 10%. Upon reaching the UTS point, mechanical instability takes place in all the structures. Gr11 (both uniaxial and biaxial tensions), PHexOct (both x and y uniaxial tensions), C41 (biaxial tension), Gr10 (biaxial tension), and SqGr13 (y-uniaxial and biaxial tension) underwent brittle fracture with a sudden drop in stress magnitudes after the UTS point. The remainder of the allotropes showed a slow and smooth decrease in stress against increasing magnitudes of strain.

We utilized Eqs. (2)–(10) for fitting the stress-strain data until the maximum 2nd P–K stress point (i.e. the UTS point). The second-order nonlinear elastic constants thus obtained were utilized to calculate  $E$  and Poisson's ratio ( $\nu$ ) using the following equations

$$E = \frac{C_{11}^2 - C_{12}^2}{C_{11}}, \quad \nu = \frac{C_{12}}{C_{11}}. \quad (11)$$

The magnitudes of  $E$  and UTS of the graphene allotropes are presented in Table 2. Compared to graphene, all the allotropes were found to have inferior values of UTS and Young's modulus. As expected, graphene was found to have the largest Young's modulus (348.6 N/m) among all the structures; while Gr10 possessed the lowest  $E$  of 26 N/m. Interestingly, C41, OcGr, PHexOct, graphyne, Gr10, and Gr11 was found to withstand slightly higher elongation at

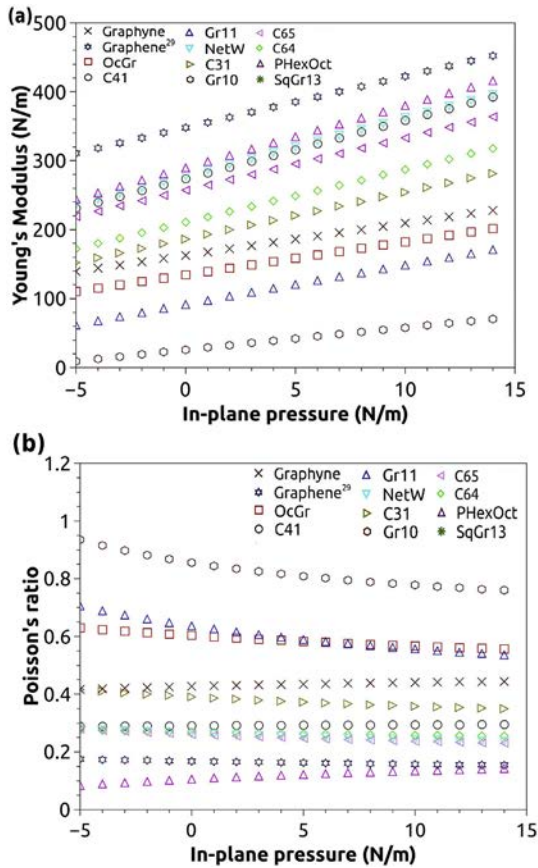


Fig. 4. (a) The Young's modulus and (b) Poisson's ratio as a function of the in-plane pressure. (A colour version of this figure can be viewed online.)

peak stress ( $\eta_u$ ) than graphene under  $y$ -uniaxial tension. Gr10 was also found to withstand slightly higher elongation at peak stress ( $\eta_u$ ) than graphene under  $x$ -uniaxial tension. For  $x$ -uniaxial tension, the magnitude of UTS for Gr10 predicted by our simulations is 37% of graphene with an area density half of graphene. These results hint towards the dependence of mechanical properties (such as UTS and  $E$ ) on different geometrical structures in graphene allotropes. This effect is discussed in detail in Section 3.4.

We observed that for all the structures the analytical fit predicted using Eqs. (2)–(10) were deviated from the 2nd P–K stress data in the post-peak regime. This mismatch at high strains can be due to the development of phonon instabilities, which has been known to dominate the failure in graphene at temperatures lower than half of its Debye temperature [33]. Since phonon instability in graphene occurs for stresses larger than its UTS [33], we assumed similar behavior for the graphene allotropes. However, rigorous investigation of the post-UTS behavior is recommended for future studies.

### 3.2. Nonlinear elastic constants

The fifteen nonzero independent elastic constants of different graphene allotropes are presented in Table 3. The third order elastic constants ( $C_{111}$ ,  $C_{222}$ ,  $C_{112}$ ) are negative for all the allotropes, which lead to mechanical softening of the structures at large strains. Excluding SqGr13, the magnitudes of  $C_{11}$  and  $C_{22}$  are of the same order for all the other allotropes, implying isotropic mechanical behavior along the  $x$  and  $y$  direction. For SqGr13,  $C_{11}$  was found to be 222.3 N/m and  $C_{22}$  was 373.4 N/m, which suggests significant anisotropic mechanical properties along the in-plane directions.

The difference in UTS values of SqGr13 for uniaxial loading in the  $x$  and  $y$  directions was found to be 11 N/m, which is the largest difference among all the structures. In the Supporting Information, we have compared the second order nonlinear elastic constants obtained from the energy-strain curve for all allotropes, and find good agreement with the results presented in Table 3 from the continuum model. We also compare the nonlinear elastic constants of graphene allotropes with other engineering materials, e.g. copper [34], aluminium [35], and graphite/epoxy [36]. Due to a stronger interaction in covalent bonds than in metallic bonding, graphene allotropes are typically stiffer than metals, reflected by a higher  $C_{11}$  and  $C_{22}$  than copper and aluminium.

The coefficients of the second ( $C_{11}$  and  $C_{22}$ ) and the third order ( $C_{111}$  and  $C_{222}$ ) terms for the different allotropes are shown in Fig. 3 (a) and (b), respectively. It can be observed that graphene and Gr10 possess the highest and lowest magnitudes of  $C_{11}$  and  $C_{22}$ , respectively. This observation is consistent with the fact that Gr10 has the lowest UTS and Young's modulus while graphene has the largest UTS and Young's modulus among all the allotropes studied here. Our simulations show a strong inverse correlation between the second and third order nonlinear elastic constants.

The pressure-dependent second-order elastic moduli ( $\tilde{C}_{11}$ ,  $\tilde{C}_{22}$ ,  $\tilde{C}_{12}$ ) of the allotropes as a function of the in-plane pressure ( $P$ ) are given by Ref. [37]:

$$\tilde{C}_{11} = C_{11} - (C_{111} + C_{112}) \frac{1 - \nu}{E} P, \quad (12)$$

$$\tilde{C}_{12} = C_{12} - C_{112} \frac{1 - \nu}{E} P. \quad (13)$$

where  $P$  is the pressure acting in the plane of the graphene allotrope,  $P_{mn} = -P\delta_{mn}$ ,  $\delta_{mn}$  is the Kronecker-delta function. It can be seen from Eqs. (12) and (13) that  $C_{112}$  couples  $\tilde{C}_{12}$  and  $\tilde{C}_{11}$  with the in-plane pressure, and, an increased pressure increases the magnitude of  $\tilde{C}_{12}$  and  $\tilde{C}_{11}$  because  $C_{111}$  and  $C_{112}$  are negative coefficients. We studied the effect of pressure on  $E$  and  $\nu$ , which is presented in Fig. 4 (a) and (b), respectively. The Young's modulus increases linearly in all the allotropes as a function of pressure. The rate of increase in  $E$  is smaller in allotropes with  $sp$  bonds (graphyne, SqGr13, and Gr10) compared to the allotropes with  $sp^2$  bonds. For most allotropes, the absolute value of Poisson's ratio decreases with an increasing in-plane pressure. Interestingly, the Poisson's ratio of Gr10 is larger than 0.5. This is a unique characteristic of 2D materials due to the invariance of the thickness during deformation [15]. While graphene was found to possess the highest Young's modulus, Gr10 possessed the lowest Young's modulus (Fig. 4(a)). However, an opposite trend was observed in Poisson's ratio on these two materials (Fig. 4(b)). These results suggest that allotropes with different geometrical structures tend to have different Young's moduli and Poisson's ratios. These relations between the geometrical structures and mechanical properties were explored further in Section 3.4.

### 3.3. Relationship between UTS and the strain corresponding to UTS point $\eta_u$

Fig. 5 (a)–(c) show the relationship between UTS and  $\eta_u$  for the allotropes. We derive the following observations from these figures. The calculated UTS values for all the graphene allotropes are found to be inferior compared to graphene (See Fig. 5 (a)–(c), Table 2). Gr10 has the lowest UTS of 11 N/m, which is approximately 30 N/m lower than that of graphene. Also, under uniaxial tension,  $\eta_u$  for some allotropes (Gr11, C41, OcGr, Gr10, and PHexOct) is larger than that of graphene. However, most of the allotropes possess higher

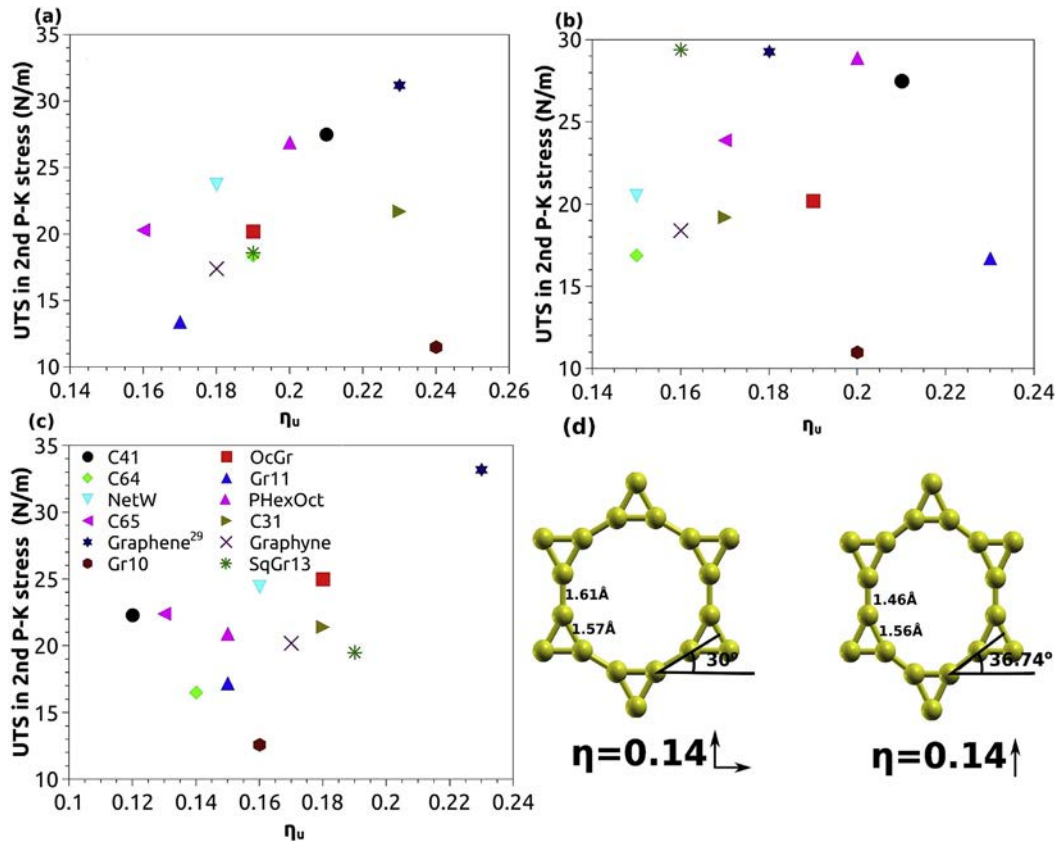


**Fig. 5.** Variation of UTS and corresponding  $\eta_u$  for all allotropes under study: (a) uniaxial tension in the x direction, (b) uniaxial tension in the y direction, and (c) biaxial tension. (d) Illustration of the difference in bond angle and bond length for Gr11 at  $\eta = 0.14$  for both biaxial and y-uniaxial tension. Clearly the angular deviation due to uniaxial stretching is found to be much larger than biaxial tension, and the bond length is much shorter. (A colour version of this figure can be viewed online.)

magnitudes of  $\eta_u$  under uniaxial tension when compared to biaxial tension. For instance, Gr11 has  $\eta_u = 0.23$  under y-uniaxial tension (Fig. 5(b) and Table 2), but with only 0.15 for biaxial tension (Fig. 5(c) and Table 2).

The increase in  $\eta_u$  under uniaxial tension compared to biaxial tension can be due to the increased bond rotation in carbon rings. Under biaxial tension, bonds do not rotate but are stretched. However, under uniaxial tension, those bonds not parallel or perpendicular to the loading direction undergo rotation. Bond rotation enables the relaxation of bond stretching, leading to an increase in the  $\eta_u$  during uniaxial tension. For example in Fig. 5(d), we show the structure of Gr11 at a strain of 0.14 for both y-uniaxial and biaxial tension. The bond rotation angle for y-uniaxial tension ( $36.74^\circ$ ) is larger than biaxial tension ( $30^\circ$ ). Due to this rotation, the bond strain is partially relaxed. As a result, the bond lengths of Gr11 under y-uniaxial tension (1.46 Å and 1.56 Å) are smaller than that under biaxial tension (1.61 Å and 1.57 Å).

These observations suggest that the topological arrangement of carbon atoms in graphene allotropes are of significant importance in determining their mechanical properties. In the following section, we search for quantitative relationships between geometric parameters and mechanical properties such as the UTS, Young's modulus and Poisson's ratio in these systems.

### 3.4. Analysis of structure-property relationships

#### 3.4.1. Physical insights into mechanical properties

Different topological arrangements of carbon atoms in monolayers give rise to graphene allotropes, therefore, their mechanical properties are related to the underlying atomic architecture and the

hybridization of the C-C bonds in the structure. The mechanics of these structures are described by the interactions between individual atoms, which may be characterized by a force field based on classical mechanics. According to molecular mechanics theory, this force field depends on relative positions of individual atoms. When a structure is deformed, the energy stored in the structure is a sum of several individual energy sources, e.g. bond stretch, bond rotation, dihedral angle torsion, out of plane torsion, and van der Waals interactions. The total stored energy in the whole system can be expressed as [38].

$$\Delta U = \Delta U_r + \Delta U_\theta + \Delta U_\phi + \Delta U_\omega + \Delta U_{vdw}, \quad (14)$$

where  $\Delta U_r$ ,  $\Delta U_\theta$ ,  $\Delta U_\phi$ ,  $\Delta U_\omega$ , and  $\Delta U_{vdw}$  represent the energy increase due to bond stretching, bond angle bending, dihedral angle torsion, out of plane torsion, and non-bonded van der Waals interaction. It is known that the van der Waals interactions produce weak attractive forces and therefore it is assumed that the contribution of van der Waals interactions to the total potential energy is negligible compared to rest of the components in Eq. (14) [39,40]. In our simulations, during deformation, all carbon atoms remain coplanar. Therefore, apart from  $\Delta U_r$  and  $\Delta U_\theta$ , the rest of the energy contributions are negligible. Hence Eq. (14) can be rewritten as

$$\Delta U(\eta) = \Delta U_r(\eta) + \Delta U_\theta(\eta). \quad (15)$$

The first derivative of energy with strain ( $\partial \Delta U_1(\eta_1)/\partial \eta_1$  or  $\partial \Delta U_2(\eta_2)/\partial \eta_2$ ) is proportional to the normal stress ( $\sigma_{11}$  or  $\sigma_{22}$ ). The second derivative ( $\partial^2 \Delta U_1(\eta_1)/\partial \eta_1^2|_{\eta_1=0}$  or  $\partial^2 \Delta U_2(\eta_2)/\partial \eta_2^2|_{\eta_2=0}$ ) is proportional to the corresponding second order nonlinear elastic

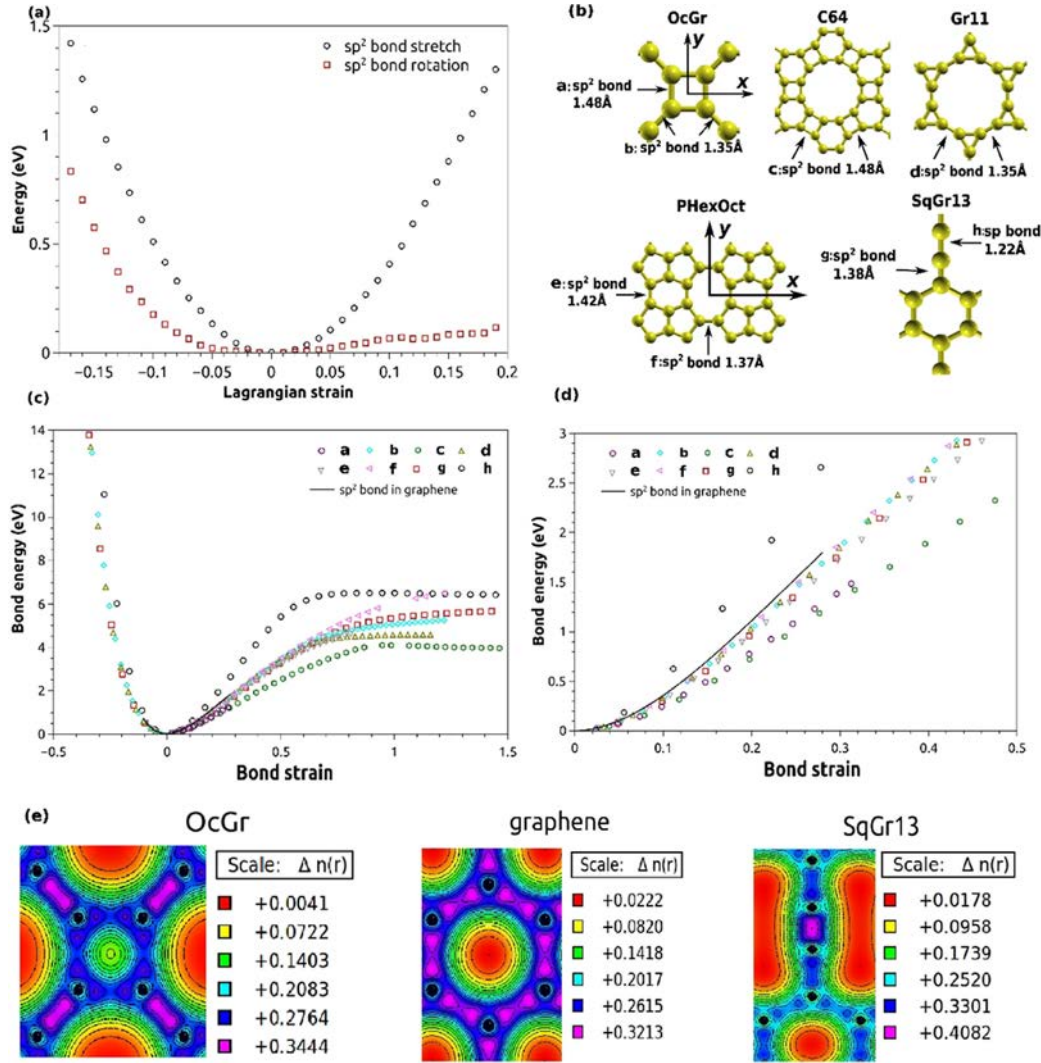


**Fig. 6.** (a)  $\Delta U_\theta(\eta)$  for the unit cell of graphene and  $\Delta U_r(\eta)$  of one bond in graphene in uniaxial tension along the x direction. (b) Illustration of different  $sp^2$  and  $sp$  bonds used for the calculation of  $\Delta U_r(\eta)$ . The bond labels in (b) are used for the legend entries in (c) and (d). (c)  $\Delta U_\theta(\eta)$  for different bonds shown in (b). (d)  $\Delta U_r(\eta)$  in the strain range from 0 to 0.5 which is the region highlighted in (c). (e) Charge density plot for OcGr, graphene, and SqGr13 at zero strain. (A colour version of this figure can be viewed online.)

constants ( $C_{11} = \partial\sigma_{11}/\partial\eta_1|_{\eta_1=0}$  and  $C_{22} = \partial\sigma_{22}/\partial\eta_2|_{\eta_2=0}$ ). In the next few sections we discuss the effect of several geometrical factors on  $\Delta U(\eta)$  and Poisson's ratio of the allotropes. Subsequently, we establish relationships between structure and mechanical properties.

**3.4.1.1. Energetics of bond deformation.** According to Eq. (15), the energy stored during the deformation of graphene allotropes is a sum of  $\Delta U_r$  and  $\Delta U_\theta$ . In order to decouple the influence of  $\Delta U_r$  and  $\Delta U_\theta$ , we calculated  $\Delta U(\eta)$  for graphene under uniaxial and biaxial deformation. In graphene all the  $sp^2$  bonds are of identical length and bond angle (3 bonds per representative unit cell). As a result, during biaxial deformation, they are equally stretched or compressed with no bond rotation. Therefore, for biaxial loading,  $\Delta U(\eta)$  of the unit cell can be written as

$$\Delta U(\eta) = \sum_{i=1}^3 \Delta U_r^{sp^2}(\eta_r^i) = 3\Delta U_r^{sp^2}(\eta), \quad \eta_r^1 = \eta_r^2 = \eta_r^3 = \eta, \quad (16)$$

where  $\eta_r^i = (l' - l_0)/l_0$  is the Lagrangian strain in the  $i$ -th bond,  $l_0$  is the initial length and  $l'$  is the bond length for an externally applied strain of  $\eta$ . During uniaxial tension in the zigzag direction, both

bond stretch and bond rotation occur. We calculated  $\Delta U_\theta^{sp^2}$  for the unit cell of graphene under uniaxial tension by using the magnitudes of  $\Delta U_r^{sp^2}(\eta_r^i)$  of the same bond under biaxial tension calculated using Eq. (16), with strain values equal to the corresponding bond strain in uniaxial tension. Therefore,  $\Delta U_\theta^{sp^2}$  in the unit cell of graphene is given by,  $\Delta U_\theta^{sp^2} = \Delta U(\eta) - \sum_{i=1}^3 \Delta U_r^{sp^2}(\eta_r^i)$ . In Fig. 6(a), we have plotted both  $\Delta U_r^{sp^2}$  and  $\Delta U_\theta^{sp^2}$  as a function of  $\eta$ , the applied uniaxial lagrangian strain. It can be seen that, for small magnitudes of strain, linear relation between stress and strain is valid. However, as discussed in Section 3.1, nonlinear elastic behavior becomes dominant as the magnitude of applied strain is increased. Interestingly, the magnitude of  $\Delta U_\theta^{sp^2}$  is significantly smaller than  $\Delta U_r^{sp^2}(\eta)$ . This implies, for a certain amount of work done by the tensile deformation of a  $sp^2$  bonded graphene allotrope, the amount of energy stored by bond stretching is significantly larger than the elastic energy retained by bond rotation. However,  $\Delta U_\theta^{sp^2}$  increases dramatically in compression ( $\Delta\theta < 0^\circ$ ) due to Pauli repulsion at short interatomic distances by the overlap of electron orbitals.

**3.4.1.2. Mechanical behavior of C-C bonds.** In order to understand the mechanical behavior of C-C bonds, we studied the sp and the sp<sup>2</sup> hybridized bonds in the graphene allotropes (each allotrope possesses different bond lengths and bond angles) under tensile and compressive loading, as shown by arrows in Fig. 6(b). Targeted uniaxial tensile and compressive tests were performed on the allotropes using the methodology described earlier. Strains were imposed only on these particular bonds shown by the arrows in Fig. 6(b), which are parallel to the loading direction. Atoms belonging to the rest of the bonds in the allotropes were frozen. In Fig. 6(c), we compared  $\Delta U_r$  for the sp<sup>2</sup> bonds in graphene with the sp bond in SqGr13, as well as the sp<sup>2</sup> bonds in OcGr, SqGr13, Gr11, PHexOct, and C64. When only one bond is stretched with no bond rotation,  $\Delta U(\eta) = \Delta U_r(\eta)$ . The form of  $\Delta U_r(\eta)$  in Fig. 6(c) is similar to that of the Lennard-Jones potential, in which the steep increase in energy at negative bond strains originate from Pauli repulsion and the rather slow increase in energy for positive bond strains originate from the attractive forces between atoms. As can be seen in Fig. 2, the maximum strains that the graphene allotropes can withstand are smaller than 0.3, and as can be seen in Fig. 6(c), after this strain the atoms in different bonds still experience attractive forces and therefore  $\Delta U_r$  keeps increasing. However, after a certain level of strain the carbon atoms are too far away from each other and therefore the electrons do not interact anymore. As a result,  $\Delta U_r$  does not change with increasing strain at this strain level.

We calculated the second order derivative of  $\Delta U_r(\eta)$  at zero strain ( $\partial^2 \Delta U_r(\eta) / \partial \eta^2 |_{\eta=0}$ ) for all the allotropes. Under a linear approximation, these terms are analogous to the stiffness constant of a linear spring, and are represented as  $K^{sp}$  and  $K^{sp^2}$  for the sp and sp<sup>2</sup> bonds in the graphene allotropes. The equilibrium bond length (i.e. bond length at zero strain) of the sp<sup>2</sup> bonds in graphene is 1.42 Å and the magnitude of  $K^{sp^2}$  is 43.68 eV. In SqGr13 (1.38 Å), Gr11 (1.35 Å), and PHexOct (1.37 Å) the length of the sp<sup>2</sup> bonds are shorter than that of graphene (1.42 Å), and the magnitudes of  $K^{sp^2}$  are 37.45 eV, 40.65 eV, and 42.29 eV, respectively. As a result, the values of  $\Delta U_r(\eta)$  for these allotropes overlap for  $\eta < 0.5$  (see

bonds with similar absolute value of initial bond strains underpins our observations of the values of  $K^{sp^2}$  in different allotropes. The variations in charge density between initially contracted and stretched bonds is directly correlated to the values of  $K^{sp^2}$  of the bond, with compressed bonds possessing a  $K^{sp^2}$  similar to graphene and stretched bonds exhibiting lower  $K^{sp^2}$  due to a much lower charge density. This observation is valid for all the sp<sup>2</sup> bonds present in the graphene allotropes studied here. Please see the [Supporting Information](#) for similar comparisons of sp<sup>2</sup> bonds in other graphene allotropes.

The  $K^{sp}$  for the sp bond in SqGr13 ( $\partial^2 \Delta U_r^{sp}(\eta) / \partial \eta^2 |_{\eta=0} = 67.72 \text{ eV}$ ) is much higher than all sp<sup>2</sup> bonds in all the structures studied here. It is well known that the energies associated with the electrons in the s orbitals are lower than the electrons in the p orbitals for any given quantum number. As a result, the electrons in s orbitals are held more closely to the nucleus than electrons in the p orbitals. Generally, the more s character a bond has, the shorter and stronger the bond will be. In SqGr13, at the center of the sp bond the charge density is equal to  $\approx 0.41 \text{ \AA}^{-2}$  which is 20% larger than that of the sp<sup>2</sup> bonds in graphene. Since each carbon atom has the same amount of electrons, a severe concentration of electrons in the sp bond decreases the charge density in the nearby sp<sup>2</sup> in SqGr13, which would effectively decrease its  $K^{sp^2}$ .

**3.4.1.3. Relation between mechanical strength and area density.** The second order nonlinear elastic constants are important in determining the Young's modulus and Poisson's ratio. In this section, using mathematical derivations, we demonstrate how different topological arrangements lead to variations in the second order nonlinear elastic constants in graphene allotropes and thereby influence their Young's modulus and Poisson's ratio. Let us consider a 2D graphene allotrope consisting of sp and sp<sup>2</sup> bonds. For small strains, the stored energy of the whole system is given by:

$$\Delta U(\eta) = \Delta U_r^{sp}(\eta) + \Delta U_r^{sp^2}(\eta) + \Delta U_\theta = \sum_{i=1}^n \Delta U_r^{sp}(\eta_i) + \sum_{j=1}^m \Delta U_r^{sp^2}(\eta_j) + \Delta U_\theta, \quad (17)$$

Fig. 6(d)). For the allotropes with sp<sup>2</sup> bonds longer than graphene, the magnitude of  $K^{sp^2}$  is significantly smaller than graphene. For example, the sp<sup>2</sup> bond in C64, which belongs to the square rings (shown by arrows in Fig. 6(b)) has a bond length of 1.48 Å, and its  $K^{sp^2}$  is 29.33 eV which is significantly smaller than graphene. In order to understand the difference in  $K^{sp^2}$  for different bonds, let us consider the case of OcGr which has two different types of sp<sup>2</sup> bonds, one with an equilibrium bond length of 1.48 Å, i.e. 4% longer than the sp<sup>2</sup> bond in graphene, and the other with the bond length of 1.35 Å, i.e. 5% shorter than the sp<sup>2</sup> bond in graphene. The spring constants of these sp<sup>2</sup> bonds in OcGr are 41.32 eV and 31.14 eV, respectively. In Fig. 6(e), we have plotted the charge densities of the sp<sup>2</sup> bonds in OcGr, graphene and SqGr13. The charge density at the center of the sp<sup>2</sup> bonds in graphene is approximately  $0.32 \text{ \AA}^{-2}$ . It can be seen that, in OcGr, the charge density at the center of the longer sp<sup>2</sup> bond is approximately  $0.28 \text{ \AA}^{-2}$ , which is 16% smaller than graphene. On the other hand the charge density at the center of the shorter bond is approximately  $0.34 \text{ \AA}^{-2}$ , which is only 7% larger than graphene. This difference in the charge density for

$$\Delta U(\eta) = \sum_{i=1}^n \frac{1}{2} K_i^{sp} (\eta_i^{sp})^2 + \sum_{j=1}^m \frac{1}{2} K_j^{sp^2} (\eta_j^{sp^2})^2 + \Delta U_\theta. \quad (18)$$

where  $\Delta U_r^{sp}(\eta_i)$  and  $\Delta U_r^{sp^2}(\eta_j)$  represent the energy of the  $i$ -th sp and  $j$ -th sp<sup>2</sup> bond under bond strains of  $\eta_i$  and  $\eta_j$ , respectively. Also,  $n$  and  $m$  are the total number of sp and sp<sup>2</sup> bonds in the structure. Applying average inequality to the first two terms in the right hand side of Eq. (18), we get

$$\sum_{i=1}^n \frac{1}{2} K_i^{sp} (\eta_i^{sp})^2 + \sum_{j=1}^m \frac{1}{2} K_j^{sp^2} (\eta_j^{sp^2})^2 \geq \frac{1}{2} (n+m) (\sqrt{K_{\text{eff}}} \eta_{\text{eff}})^2, \quad (19)$$

where  $K_{\text{eff}}$  and  $\eta_{\text{eff}}$  are the effective second order derivative of the bond energy increase and effective strains for all the bonds in the structures, respectively. Now, the minimum in  $\Delta U(\eta)$  will be

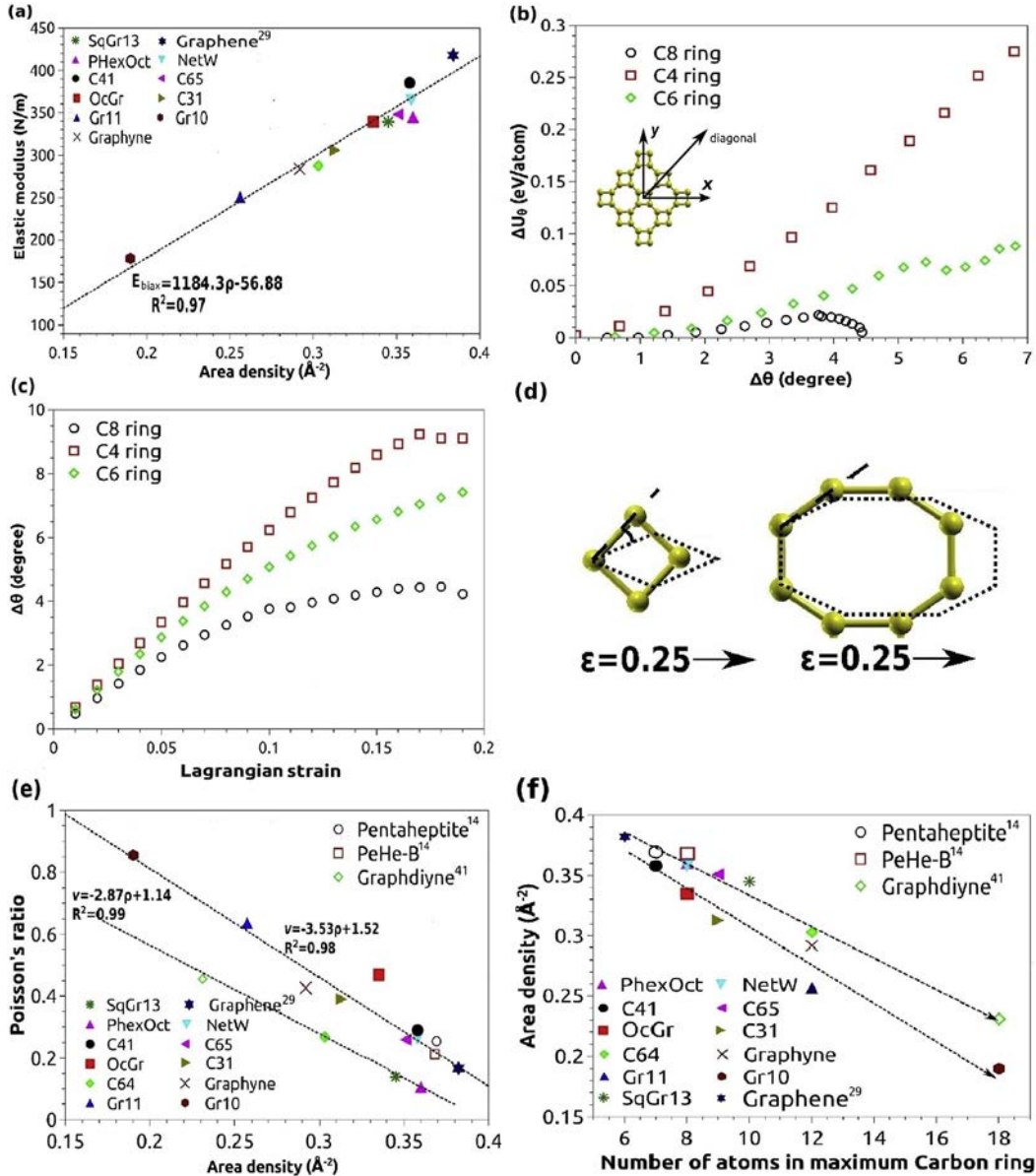


Fig. 7. (a) Relations between area density and the  $E_{\text{biax}}$  in biaxial tension. (b)  $\Delta U_\theta$  as a function of  $\theta$  during tension. (c) angle change as a function of tensile strain. (d) Illustration of different bond angle deviation for carbon rings under the same strain. It is obvious that C8 has a much lower angle deviation than C4. (e) The relation between the area density and Poisson's ratio. (f) The relation between the area density and the number of atoms in the maximum carbon ring. (A colour version of this figure can be viewed online.)

achieved when

$$\sqrt{K_j^{sp^2} \eta_j^{sp^2}} = \sqrt{K_i^{sp} \eta_i^{sp}}, i = 1, 2, 3 \dots n, j = 1, 2, 3 \dots m. \quad (20)$$

This condition implies that under linear approximation, during deformation,  $\Delta U(\eta)$  for the entire structure will be minimized when the energy increase for each participating bond is the same. That is to say,  $\Delta U(\eta)$  reaches its minimum ( $\Delta U(\eta)_{\text{min}}$ ) value when all the bonds can be replaced by the same number of equivalent bonds with the same strain  $\eta_{\text{eff}}$ , and no bond rotation occurs ( $\Delta U_\theta = 0$ ). Therefore, we write

$$\Delta U(\eta)_{\text{min}} = \frac{1}{2} K_{\text{eff}} \cdot (n + m) \cdot (\eta_{\text{eff}})^2. \quad (21)$$

In biaxial tension, the unit cell of graphene allotropes is equally stretched in all the directions, there is no particular loading

direction and all the bonds can stretch to fit Eq. (20), regardless of their individual orientations. However, in uniaxial tension, strain in the bonds perpendicular and parallel to the loading direction can not be the same. Therefore, Eq. (20) is not valid for uniaxial tensile deformation.

In biaxial tension, the hydrostatic stress for a 2D material for small magnitudes of  $\eta$  is given by

$$P = \frac{1}{2} (\sigma_{11} + \sigma_{22}) = \frac{1}{2} \left( \sum_1 + \sum_2 \right) \approx \frac{1}{2} (C_{11} + C_{12}) \eta + \frac{1}{2} (C_{22} + C_{12}) \eta = E_{\text{biax}} \eta. \quad (22)$$

where  $E_{\text{biax}}$  is the modulus of biaxial tension. The energy increase per unit area by the hydrostatic stress is

**Table 4**

Prediction of mechanical properties based on Eq. (27) (second order nonlinear elastic constants, Young's modulus, Poisson's ratio, UTS, and corresponding strain) of different graphene allotropes. P represents prediction results from our equations and S represents simulation results from DFT.

Graphene allotropes	Poisson's ratio		Young's modulus (N/m)		Second order nonlinear elastic constants (N/m)					
	Prediction	Simulation	Prediction	Simulation	C <sub>12</sub> (P)	C <sub>12</sub> (S)	C <sub>22</sub> (P)	C <sub>22</sub> (S)	C <sub>11</sub> (P)	C <sub>11</sub> (S)
Graphene	0.16	0.17	331.8	348.6	56	60	341	358	341	358
Gr11	0.61	0.64	93.9	92.6	94	98	152	152	152	154
OcGr	0.33	0.6	226.7	134.5	85	128	255	212	255	212
C64	0.27	0.27	219.7	210	64	61	237	227	237	227
C41	0.26	0.29	270.6	272.9	79	87	292	298	292	299
NetW	0.11	0.26	326.1	277.9	36	79	330	273	330	299
PHexOct	0.11	0.11	330.1	289.9	36	31	334	335	334	293
C65	0.28	0.26	257.7	257.2	79	72	280	277	280	276
C31	0.41	0.18	210.6	186.8	105	86	254	220	254	220
Graphyne	0.3	0.43	201.8	162.1	67	85	222	199	222	199
Gr10	0.85	0.86	25.8	26	77	83	91	94	91	97
SqGr13	0.15	0.14	298.6	203.5	46	42	305	373	305	222

$$\frac{C_{11} + 2C_{12} + C_{22}}{4} \eta^2 = \frac{\Delta U(\eta)_{min}}{A} = \frac{1}{2} K_{eff} \cdot \left( \frac{n}{A} + \frac{m}{A} \right) \cdot (\eta_{eff})^2, \quad (23)$$

where  $A$  is the total area of the structure. When the applied strain,  $\eta$  ( $\eta_{eff} = \eta$ ) is small, there is no strain concentration (which is the case in the linear elastic regime). Therefore,

$$\frac{C_{11} + 2C_{12} + C_{22}}{4} = \frac{1}{2} K_{eff} \cdot \left( \frac{n}{A} + \frac{m}{A} \right). \quad (24)$$

For allotropes with only  $sp^2$  bonds, Eq. (23) can be written as

$$\frac{C_{11} + 2C_{12} + C_{22}}{4} = \frac{1}{2} K_{eff}^{sp^2} \cdot \frac{m}{A} = \frac{1}{2} K_{eff}^{sp^2} \cdot \rho_{bond} = \frac{1}{2} K_{eff}^{sp^2} \cdot \frac{3}{2} \rho_{atom}, \quad (25)$$

where  $\rho_{bond}$  is the bond density, which is proportional to area density,  $\rho_{atom}$ .

For allotropes with both  $sp$  and  $sp^2$  bonds, Eq. (24) becomes

$$\frac{C_{11} + 2C_{12} + C_{22}}{4} = \frac{1}{2} K_{eff} \cdot \left( \frac{n}{A} + \frac{m}{A} \right) = \frac{1}{2} K_{eff} \cdot \rho_{bond}, \quad (26)$$

In order to assess the suitability of Eq. (25), in Fig. 7(a), we plotted the biaxial tensile elastic moduli of all the allotropes (extracted from our continuum model presented in Table 3) as a function of  $\rho_{atom}$ . The dotted line shows the linear fit to the data. A linear relation ( $E_{biax} = A\rho_{atom} - B$ ) with  $R^2$  exceeded 0.97 exists for all the graphene allotropes, including those with  $sp$  bonds, irrespective of structural isotropy. The fitting parameter  $A$  has the energy unit (here the unit is  $10^{-20}$  J) and  $B$  has the same unit of force per unit length (in the current study the unit is N/m). In our study,  $E_{biax} = 1184.3\rho_{atom} - 56.88$ . A minimal area density is required for the formation of a covalent bond, which is captured here, as  $E_{biax} \rightarrow 0$ , when  $\rho_{atom} > 0$ .

**3.4.1.4. Physical insights into Poisson's ratio.** The Poisson's ratio offers a fundamental criterion to judge a material's resistance to distort under mechanical load in the lateral direction instead of changing its volume when deformed in the elastic regime. Under uniaxial loading, structures with a positive Poisson's ratio (which is the case for all the allotropes studied here) contract in the direction perpendicular to the loading direction. Without bond rotation, the graphene allotropes can not deform in this direction. In Section 3.4.1.1, we showed that  $\Delta U_\theta$  increased dramatically during compression due to Pauli's repulsive forces. As the size of the carbon ring increases, the distance between the center of the ring and

the carbon atoms of the ring increase. As a result, the charge density at the center of the ring becomes very small. For the graphene allotropes studied here, the charge density at the center becomes almost zero for the carbon rings with more than 7 atoms. The smaller the carbon ring, the closer the electrons in different carbon atoms of the ring are to each other during a contraction and therefore more difficult it is for the bonds in small carbon rings to undergo rotation. As a result, as the size of the carbon ring becomes smaller, a larger amount of energy is required to produce  $\Delta\theta$ . In Fig. 7 (b), we compared  $\Delta U_\theta$  per atom as a function of  $\Delta\theta$  for C4, C8 in OcGr, and C6 ring in graphene. Uniaxial tension along the  $x$ -direction caused the deformation of the C8 ring in OcGr, while uniaxial tension in the direction aligned at  $45^\circ$  with the  $x$ -direction (shown as a diagonal direction in Fig. 7(b)) results in the deformation of the C4 ring. It can be seen that the energy required to produce the same  $\Delta\theta$  is comparatively larger for the smallest ring (i.e. C4). The second order derivative of  $\Delta U_\theta$  with  $\Delta\theta$ , which is the stiffness constant for bond rotation, is almost zero for the C8 carbon ring. Consequently, the magnitude of Poisson's ratio will be larger for allotropes with larger rings.

In addition to Pauli repulsion effects, larger carbon rings have more atomic bonds, which can better distribute the total imposed strain in comparison to smaller carbon rings. With more bonds stretched and rotated, the strain and rotation per bond are smaller for larger carbon rings. As a result, although it is energetically expensive for smaller carbon rings to rotate, their average bond angle deviation and bond elongation are still higher than that of large carbon rings at the same applied strain. This effect can be seen in Fig. 7(c), where  $\Delta\theta$  is plotted as a function of applied lagrangian strain for C8 ring, C4 ring in OcGr, and C6 ring in graphene. As shown in the figure, the C4 carbon ring undergoes the largest bond rotation. In Fig. 7(d) we show the deformed C8 and C4 rings for a uniaxial tensile strain of 0.25. It is evident that the C8 ring reaches the same strain level with smaller bond angle rotation and bond stretch compared to the C4 ring. Consequently, graphene allotropes comprised of more large carbon rings always experience a lower specific energy increase per atom and undergo bond rotation more easily, resulting in a lower second order nonlinear elastic constants during uniaxial tension. Therefore, based on the definition of Poisson's ratio ( $\nu = C_{12}/C_{11}$ ), the magnitude of the Poisson's ratio will be higher for allotropes with larger rings. In the allotropes studied here, large carbon rings are always tessellated next to small carbon rings. Due to traction compatibility, bond rotation therefore occurs in both small and large rings. Therefore, the influence of the large carbon rings on the Poisson's ratio is weakened by the presence of other small carbon rings in each allotrope.

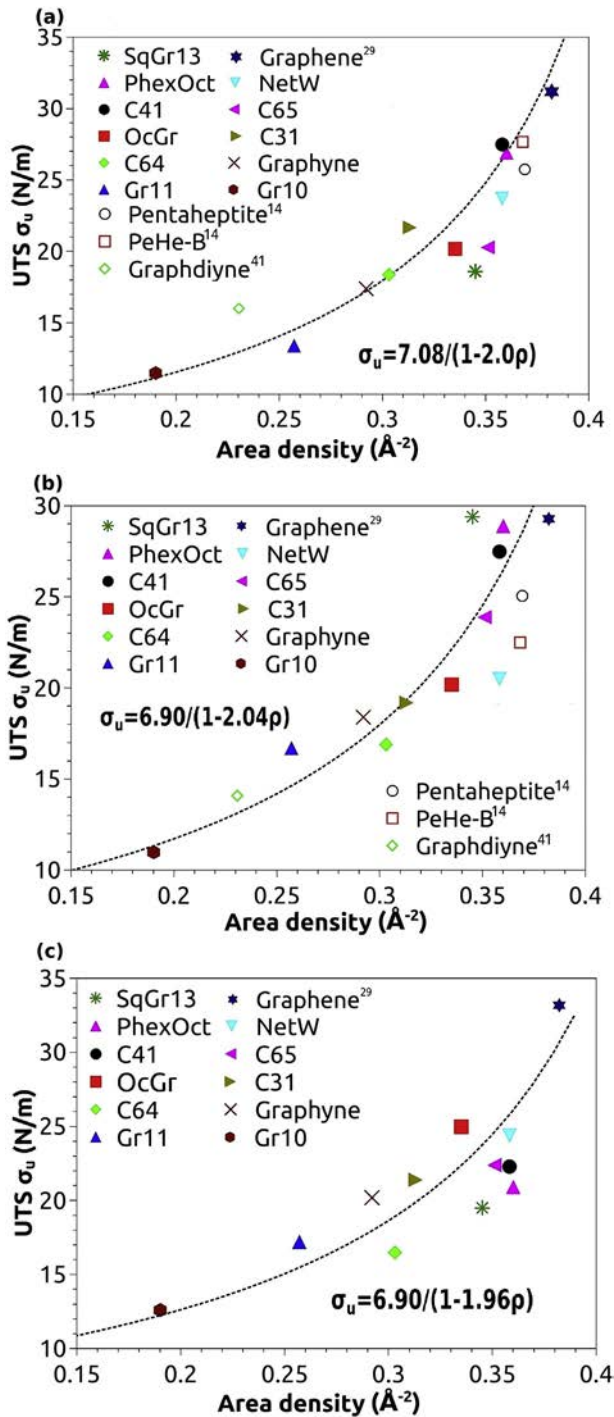


**Fig. 8.** The relationships between UTS and area density for uniaxial tension in x (a), uniaxial tension in y (b), and biaxial tension (c). (A colour version of this figure can be viewed online.)

**Table 5**

Fitting constants and standard error of the regression  $S$  for Eq. (28) UTS (N/m) for 15 allotropes.

	x-uniaxial UTS	y-uniaxial UTS	Biaxial UTS
A	2.00	2.04	1.96
B	7.08	6.90	7.55
S	1.69	2.58	2.62

### 3.4.2. Prediction of mechanical properties

**3.4.2.1. Prediction of nonlinear elastic constants, Poisson's ratio and Young's modulus.** Based on the above discussion, structures with smaller carbon rings, i.e. higher area density, have a lower propensity for contracting laterally, and possess a smaller Poisson's ratio. This effect is shown in Fig. 7(e). The dotted lines are linear fits to Poisson's ratio of all the graphene allotropes studied here, and also three graphene allotropes studied elsewhere [14,41]. The  $R^2$  value for the linear fits exceeded 0.98. It can be seen that Gr10 has the highest Poisson's ratio among all the allotropes, followed by Gr11, graphyne, C31, and C41. These allotropes follow the top dashed line in Fig. 7(e) ( $\nu = C_{12}/C_{11} = -3.53\rho_{\text{atom}} + 1.52$ ). Additionally, graphdiyne [41], C64, SqGr13, and PhexOct follow the other dashed line ( $\nu = C_{12}/C_{11} = -2.87\rho_{\text{atom}} + 1.14$ ).

Similarly, the area density of graphene allotropes decreases, but not monotonically as the size of the largest carbon ring increases (Fig. 7(f)). The existence of two linear relations between area density and the number of atoms in the largest carbon ring demonstrates the influence of other small carbon rings in the respective structures. For example, both C64 and Gr11 have identical largest carbon rings (11 atoms), however, the C4 and the C6 rings in C64 occupy a larger area (41% of the unit cell) than the C3 rings in Gr11 (7.5% of the unit cell). As a result, the fraction of area occupied by the C11 rings in Gr64 is smaller than that of Gr11, causing a higher area density in C64 ( $0.303 \text{ \AA}^{-2}$ ) than Gr11 ( $0.256 \text{ \AA}^{-2}$ ) and a lower Poisson's ratio in C64 (0.27) than Gr11 (0.64). For solely  $sp^2$  hybridized allotropes, C41, OcGr, C31, Gr11, and Gr10 are composed of one large and one small carbon ring. In these materials, area density decreases as the size of the largest carbon ring increases. They appear at the bottom dashed lines in Fig. 7(f). Other allotropes, including Pentaheptite [14], PeHe-B [14], are composed of more than two kinds of carbon rings and they occupy the top dashed line in Fig. 7(f). Generally, the structures which populate the top line in Fig. 7(f) tend to occupy the bottom line ( $C_{12}/C_{11} = -2.87\rho_{\text{atom}} + 1.14$ ) in the area density-Poisson's ratio relation in Fig. 7(e). Therefore, knowledge of the constitutive ring structures permits an *a priori* estimation of the Poisson ratio through calculation with the appropriate analytical relation ( $C_{12}/C_{11} = -3.53\rho_{\text{atom}} + 1.52$  or  $C_{12}/C_{11} = -2.87\rho_{\text{atom}} + 1.14$ ).

For isotropic materials, where  $C_{11} = C_{22}$ , we obtain the following relationships between  $C_{11}$ ,  $C_{22}$  and area density:

$$\begin{aligned} C_{11} + C_{12} &= 1184.3\rho_{\text{atom}} - 56.88, \frac{C_{12}}{C_{11}} \\ &= -3.53\rho_{\text{atom}} + 1.52 \text{ or } \frac{C_{12}}{C_{11}} = -2.87\rho_{\text{atom}} + 1.14 \end{aligned} \quad (27)$$

Eq. (27) can be used to predict  $C_{11}$  and  $C_{12}$ , and subsequently, Young's moduli and Poisson's ratios for different area densities. It should be noted that this equation set is applicable only to the isotropic 6-fold symmetric allotropes such as, C64, Gr10, Gr11, graphyne, and graphene. For other anisotropic allotropes (e.g. SqGr13), the relation between Poisson's ratio and area density is not valid and requires the shear modulus to predict the variation in Poisson's ratio for all orientations. However, Eq. (27) is still valid if  $C_{11} = C_{22}$ , and therefore, it can be used to predict the second order nonlinear elastic constants in certain orientations. In Table 4 we have listed the predicted values of second order nonlinear elastic constants, Young's modulus and Poisson's ratio obtained using Eq. (27), and compared them with the results obtained by fitting the simulated stress-strain data (see Section 3.1 and 3.2). For isotropic graphene allotropes, our predictions are in good agreement with simulated results. However, for anisotropic materials, e.g., OcGr, huge differences exist.

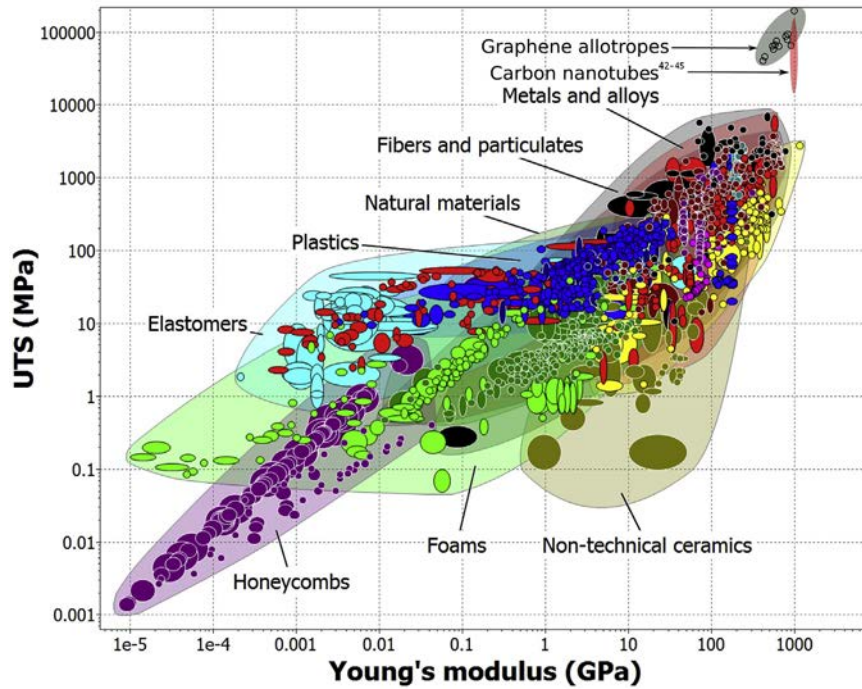


**Fig. 9.** Material property chart of Young's modulus vs. tensile strength for graphene allotropes compared with traditional engineering materials. Graphene allotropes expand the structure-property space of current material offerings and possess comparatively higher stiffnesses and strengths. (A colour version of this figure can be viewed online.)

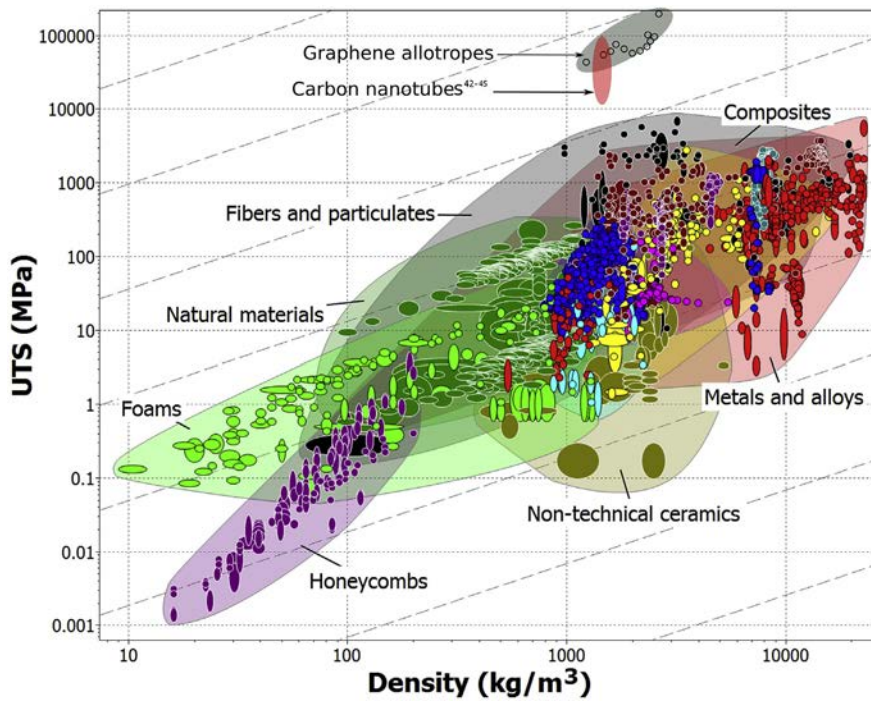


**Fig. 10.** Material property chart of UTS vs. density for graphene allotropes compared with traditional engineering materials. Graphene allotropes are found to expand the structure-property space, possessing strengths larger than any other existing material and densities in the range of many light-weight materials. (A colour version of this figure can be viewed online.)

3.4.2.2. Empirical relationship between area density and UTS. Discussions in Section 3.4.1.3 and 3.4.2.1 provide physical insights into the relationships between the area density of the allotropes and their nonlinear elastic constants, Young's modulus and Poisson's ratio. Therefore, the area density should also have an influence

on the UTS. Fig. 8 (a) to (c) show the nonlinear increase of UTS as a function of the area density for  $x$ -uniaxial tension,  $y$ -uniaxial tension, and biaxial tension, respectively. We obtained an empirical relationship to describe the relation between area density and UTS, given by

$$\sum_{\text{u}} = \frac{B}{1 - A\rho}, \quad (28)$$

where  $A(A^2)$  and  $B$  (N/m) are fitted numerical constants,  $\rho$  is the area density and  $\Sigma_{\text{u}}$  is the UTS. The estimates of  $A$ ,  $B$  and standard error of the regression coefficient  $S$  for different loading conditions are presented in Table 5. The standard error of the regression  $S$  is defined as  $S = \sqrt{\sum_{i=1}^n (x_i - x'_i)^2 / (n - 2)}$ , where  $x_i$  is the UTS for the  $i$ th allotrope;  $x'_i$  is the predicted values from Eq. (28) for the corresponding prediction UTS based on Eq. (28) for the  $i$ th allotrope.  $n$  is the total number of graphene allotropes under study. The magnitude of  $S$  for the values of UTS under three different loading conditions (i.e. uniaxial tension in  $x$  and  $y$  direction, and biaxial tension) are all smaller than 3, which is 13% of the averaged UTS for the allotropes studied here. The fitting parameters for  $x$  and  $y$  uniaxial tension were found to be similar, as expected for largely isotropic behavior along the in-plane directions.

To further test the validity and predictive capability of this empirical relation, we compared our relations with the mechanical properties of three graphene allotropes previously studied [14,41]. It can be seen from Fig. 8(a) to (c) that the predictions from Eq. (28) are also able to capture the magnitude of UTS of these materials, suggesting that Eq. (28) may be considered as a universal relation for other graphene allotropes. In the Supporting Information, we compared the predicted values of UTS with the DFT results for each graphene allotrope in a table. We note that due to the singularity problem of Eq. (28), this equations might not be valid for graphene allotropes with high area density.

### 3.5. Material selection charts

Graphene has the highest UTS and Young's modulus among all existing materials. Therefore, it is of great practical interest to investigate whether its allotropes still possess similar advantages over the traditional materials (such as polymers, composites, metals, alloys and ceramics). Fig. 9 illustrates the material property chart for Young's modulus vs. tensile strength of all known materials, where the graphene allotropes are found to reside in a sparse region inhabited by other carbonaceous materials such as graphene and carbon nanotubes [42–45]. These systems occupy an area that represents both high Young's modulus (stiffness) and large UTS. While traditional alloys and composites possess Young's moduli as high as 1000 GPa, the maximum UTS for these materials is still less than 10 GPa. In comparison, the lowest UTS in graphene allotropes is theoretically calculated to be 40 GPa, which is significantly larger than any conventional material. Although topological defects are expected to decrease the strength substantially [46–48], the specific strength of the imperfect graphene allotropes may still be sufficiently higher than traditional materials.

The material property chart for UTS vs. density is presented in Fig. 10. It can be seen that graphene allotropes possess densities in the range of 1500 Kg/m<sup>3</sup> to 2200 Kg/m<sup>3</sup>, which is similar to that of fibres and particulates. However, graphene allotropes possess UTSS approximately five to ten times greater than many materials and occupy a new area at the top of Fig. 10. Due to their impressive combination of both high UTS and stiffness at a comparatively low density, graphene allotropes have broad application prospects outside the envelope established by conventional materials.

## 4. Conclusions

Structure-property relations are important for the design and application of engineering materials. With novel 2D materials

being discovered and synthesized at an unprecedented pace, it has become important to understand their structure-mechanical property relations. In this work, we performed DFT simulations to quantify the effects of varied bonding networks in graphene allotropes. By analyzing the stress-strain responses of 11 different allotropes with varied degrees of bond hybridizations and atomic area densities, we computed the fifth order nonlinear elastic constants of their stress-strain curves based on the continuum theory. Biaxial and uniaxial tensile deformations of the sp<sup>2</sup> bonds in graphene were performed. Analysis of the energies associated with bond stretch and bond rotation revealed that the stored energy due to bond rotation is negligible compared to bond stretch energy. Further analysis demonstrated that the nonlinear elastic constants, Young's modulus and Poisson's ratio of the graphene allotropes are directly related to the area density of the atoms, irrespective of whether the structures are isotropic or anisotropic. Based on this understanding, empirical relations were obtained between area density of the allotropes and their nonlinear elastic constants, Young's moduli, Poisson's ratios and UTSS. We found that based on the size, and shape of the different carbon rings in the allotropes, all the second order nonlinear elastic constants, as well as Young's moduli and Poisson's ratios can be predicted accurately for isotropic graphene allotropes. Graphene allotropes with low area densities were found to possess a low UTS and Young's modulus, but a high Poisson's ratio. Along with pristine graphene, its allotropes were found to occupy a new area in the material-property space and surpass the mechanical properties of conventional materials.

## Acknowledgements

Financial support for this work was provided through the Natural Sciences and Engineering Research Council of Canada, and the Ontario Research Fund (ORF). The computational resources were provided by the SciNet consortium and Calcul Quebec through the Compute Canada resource allocations, and the Mitacs Globalink Scholarships. M. D. would like to acknowledge the NSERC Post-graduate Scholarship and Ontario Graduate Scholarship programs for funding. The authors also thank Prof. Tobin Filleter and Zhe Shi for important discussions.

## Appendix A. Supplementary data

Supplementary data related to this article can be found at <http://dx.doi.org/10.1016/j.carbon.2016.09.018>.

## References

- [1] G.-H. Lee, R.C. Cooper, S.J. An, S. Lee, A. van der Zande, N. Petrone, A.G. Hammerberg, C. Lee, B. Crawford, W. Oliver, J.W. Kysar, J. Hone, High-strength chemical-vapor-deposited graphene and grain boundaries, *Science* 340 (2013) 1073–1076.
- [2] D. Malko, C. Neiss, F. Viñes, A. Görling, Competition for graphene: graphynes with direction-dependent dirac cones, *Phys. Rev. Lett.* 108 (8) (2012) 086804.
- [3] S. Yadav, J. Tam, C.V. Singh, A first principles study of hydrogen storage on lithium decorated two dimensional carbon allotropes, *Int. J. Hydrog. Energy* 40 (2015) 6128–6136.
- [4] B.R. Sharma, A. Manjanath, A.K. Singh, Pentahexoctite: a new two-dimensional allotrope of carbon, *Sci. Rep.* 4 (2014) 7164.
- [5] H. Lu, S.-D. Li, Two-dimensional carbon allotropes from graphene to graphyne, *J. Mater. Chem. C* 1 (2013) 3677–3680.
- [6] M. Maruyama, S. Okada, Two-dimensional sp<sup>2</sup> carbon network of fused pentagons: all carbon ferromagnetic sheet, *Appl. Phys. Express* 6 (095101) (2013) 147–155.
- [7] V.R. Coluci, S.F. Braga, S.B. Legoas, D.S. Galvão, R.H. Baughman, Families of carbon nanotubes: graphyne-based nanotubes, *Phys. Rev. B* 68 (2003) 035430.
- [8] X.-Q. Wang, H.-D. Li, J.-T. Wang, Prediction of a new two-dimensional metallic carbon allotrope, *Phys. Chem. Chem. Phys.* 15 (2013) 2024–2030.
- [9] S.W. Cranford, D.B. Brommer, M.J. Buehler, Extended graphynes: simple scaling laws for stiffness, strength and fracture, *Nanoscale* 4 (2012)

- 7797–7890.
- [10] Q. Peng, W. Ji, S. De, Mechanical properties of graphyne monolayers: a first-principles study, *Phys. Chem. Chem. Phys.* 14 (2012) 13385–13391.
- [11] Y.Y. Zhang, Q.X. Pei, C.M. Wang, Mechanical properties of graphynes under tension: a molecular dynamics study, *Appl. Phys. Lett.* 101 (2012) 081909.
- [12] D.B. Brommer, M.J. Buehler, Failure of graphdiyne: structurally directed delocalized crack propagation, *J. Appl. Mech.* 80 (2013) 040908.
- [13] J. Zhao, N. Wei, Z. Fan, J.-W. Jiang, T. Rabczuk, The mechanical properties of three types of carbon allotropes, *Nanotechnology* 24 (2013) 095702–095712.
- [14] Z.G. Fthenakis, N.N. Lathiotakis, Graphene allotropes under extreme uniaxial strain: an *ab initio* theoretical study, *Phys. Chem. Chem. Phys.* 17 (2015) 16418–16427.
- [15] J. Hou, Z. Yin, Y. Zhang, T.-C. Chang, Structure dependent elastic properties of supergraphene, *Acta Mech. Sin.* (2016) 1–6.
- [16] A. Timoshevskii, S. Kotrechko, Y. Matviychuk, Atomic structure and mechanical properties of carbyne, *Phys. Rev. B* 91 (2015) 205407.
- [17] M. Liu, V.I. Artyukhov, H. Lee, F. Xu, B.I. Yakobson, Carbyne from first principles: chain of c atoms, a nanorod or a nanorope, *ACS Nano* 7 (2013) 10075–10082.
- [18] M.F. Ashby, *Materials Selection in Mechanical Design*, second ed., Butterworth-Heinemann, Oxford, OX; Boston, MA, 1999, pp. 111–112.
- [19] A.N. Enyashin, A.L. Ivanovskii, Graphene allotropes, *Phys. Status Solidi B* 248 (2011) 1879–1883.
- [20] X.-L. Sheng, H.-J. Cui, F. Ye, Q.-B. Yan, Q.-R. Zheng, G. Su, Octagraphene as a versatile carbon atomic sheet for novel nanotubes, unconventional fullerenes, and hydrogen storage, *J. Appl. Phys.* 112 (2012) 074315.
- [21] Q. Song, B. Wang, K. Deng, X. Feng, M. Wagner, J.D. Gale, K. Müllen, L. Zhi, Graphenylene, a unique two-dimensional carbon network with non-delocalized cyclohexatriene units, *J. Mater. Chem. C* 1 (2013) 38–41.
- [22] X.-Q. Wang, H.-D. Li, J.-T. Wang, Prediction of a new two-dimensional metallic carbon allotrope, *Phys. Chem. Chem. Phys.* 15 (2013) 2024–2030.
- [23] K.S. Novoselov, Electric field effect in atomically thin carbon films, *Science* 306 (2004) 666–669.
- [24] M.J. Bucknum, E.A. Castro, The squarographites: a lesson in the chemical topology of tessellations in 2- and 3-dimensions, *Solid State Sci.* 10 (2008) 1245–1251.
- [25] R.H. Baughman, H. Eckhardt, M. Kertesz, Structure-property predictions for new planar forms of carbon: layered phases containing sp<sup>2</sup> and sp atoms, *J. Chem. Phys.* 87 (1987) 6687–6699.
- [26] P. Giannozzi, S. Baroni, N. Bonini, M. Calandra, R. Car, C. Cavazzoni, D. Ceresoli, G.L. Chiarotti, M. Cococcioni, I. Dabo, A. Dal Corso, S. de Gironcoli, S. Fabris, G. Fratesi, R. Gebauer, U. Gerstmann, C. Gougousis, A. Kokalj, M. Lazzeri, L. Martin-Samos, N. Marzari, F. Mauri, R. Mazzarello, S. Paolini, A. Pasquarello, L. Paulatto, C. Sbraccia, S. Scandolo, G. Sclauzero, A.P. Seitsonen, A. Smogunov, P. Umari, R.M. Wentzcovitch, QUANTUM ESPRESSO: a modular and open-source software project for quantum simulations of materials, *J. Phys. Condens. Matter* 21 (2009) 395502–395520.
- [27] J.P. Perdew, K. Burke, M. Ernzerhof, Generalized gradient approximation made simple, *Phys. Rev. Lett.* 77 (1996) 3865–3868.
- [28] H.J. Monkhorst, J.D. Pack, Special points for Brillouin-zone integrations, *Phys. Rev. B* 13 (1976) 5188–5192.
- [29] X. Wei, B. Fragneaud, C.A. Marianetti, J.W. Kysar, Nonlinear elastic behavior of graphene: *Ab initio* calculations to continuum description, *Phys. Rev. B* 80 (2009) 205407.
- [30] M.A. Crisfield, *Non-linear Finite Element Analysis of Solids and Structures*, Wiley, Chichester; New York, 1991, pp. 18–19.
- [31] J.W. Schultz, R.L. Moore, Effective medium calculations of the electromagnetic behavior of single walled carbon nanotube composites, *MRS Proc.* 739 (2002). H7.42.
- [32] Q. Peng, C. Liang, W. Ji, S. De, A theoretical analysis of the effect of the hydrogenation of graphene to graphane on its mechanical properties, *Phys. Chem. Chem. Phys.* 15 (2013) 2003–2011.
- [33] F. Liu, P. Ming, J. Li, *Ab initio* calculation of ideal strength and phonon instability of graphene under tension, *Phys. Rev. B* 76 (2007) 471–478.
- [34] H.M. Ledbetter, E.R. Naimon, Elastic properties of metals and alloys. II. Copper, *J. Phys. Chem. Ref. Data* 3 (1974) 897–935.
- [35] J.F. Thomas, Third-order elastic constants of aluminum, *Phys. Rev.* 175 (1968) 955–962.
- [36] W.H. Prosser, R.E. Green, Characterization of the nonlinear elastic properties of graphite/epoxy composites using ultrasound, *J. Reinf. Plast. Compos.* 9 (1990) 162–173.
- [37] S.Y. Davydov, Third-order elastic moduli of single-layer graphene, *Phys. Solid State* 53 (2011) 665–668.
- [38] G. Odegard, Equivalent-continuum modeling of nano-structured materials, *Compos. Sci. Technol.* 62 (2002) 1869–1880.
- [39] S.K. Georgantzinos, D.E. Katsareas, N.K. Anifantis, Graphene characterization: a fully non-linear spring-based finite element prediction, *Phys. E Low-Dimens. Syst. Nanostruct.* 43 (2011) 1833–1839.
- [40] G.I. Giannopoulos, P.A. Kakavas, N.K. Anifantis, Evaluation of the effective mechanical properties of single walled carbon nanotubes using a spring based finite element approach, *Comput. Mater. Sci.* 41 (2008) 561–569.
- [41] R.C. Andrew, R.E. Mapasha, A.M. Ukpong, N. Chetty, Mechanical properties of graphene and boronitrene, *Phys. Rev. B* 85 (2012) 777–782.
- [42] S. Bellucci, Carbon nanotubes: physics and applications, *Phys. Status Solidi C* 2 (2005) 34–47.
- [43] H.G. Chae, S. Kumar, Rigid-rod polymeric fibers, *J. Appl. Polym. Sci.* 100 (2006) 791–802.
- [44] M. Meo, M. Rossi, Prediction of Young's modulus of single wall carbon nanotubes by molecular-mechanics based finite element modelling, *Compos. Sci. Technol.* 66 (2006) 1597–1605.
- [45] S.B. Sinnott, R. Andrews, Carbon nanotubes: synthesis, properties, and applications, *Crit. Rev. Solid State Mater. Sci.* 26 (2001), 145–249.
- [46] M. Daly, M. Reeve, C. Veer Singh, Effects of topological point reconstructions on the fracture strength and deformation mechanisms of graphene, *Comput. Mater. Sci.* 97 (2015) 172–180.
- [47] A. Zandiatashbar, G.-H. Lee, S.J. An, S. Lee, N. Mathew, M. Terrones, T. Hayashi, C.R. Picu, J. Hone, N. Koratkar, Effect of defects on the intrinsic strength and stiffness of graphene, *Nat. Commun.* 5 (2014) 3186.
- [48] M. Daly, C. Veer Singh, A kinematic study of energy barriers for crack formation in graphene tilt boundaries, *J. Appl. Phys.* 115 (2014) 223513.